

# Plume Impingement on a Dusty Lunar Surface

A. B. Morris, D. B. Goldstein, P. L. Varghese, L. M. Trafton

*ASE-EM Department, 1 University Station, C0600, Austin, TX 78712, USA*

**Abstract.** A loosely coupled continuum-DSMC solver is used to simulate the interaction between the exhaust from a rocket engine with the lunar surface. This problem is of particular interest because the high velocity dust spray can damage nearby structures. The flow field is challenging to simulate because continuum assumptions are no longer valid in the far field, while in the near field DSMC becomes impractical because of the high collision rate. In the current work the high density core of the rocket plume is modeled with NASA's continuum flow solver, DPLR [1]. Since the two solvers are loosely coupled, i.e. one-way coupling from the DPLR to the DSMC regimes, the interface between the two solvers is placed in the supersonic region above the surface shock. At the lunar surface, a boundary layer develops and the shear stress causes dust grains to slide and eventually enter the flow field. Robert's theory of dust entrainment [2,3] is used to predict how much dust is lofted into the flow field by the near surface flow conditions. In Robert's original theory the interaction between entrained dust grains and the gas was neglected and the particles were assumed to follow ballistic trajectories. In our current model, the dust grains are coupled with the DSMC gas model. Both the dust trajectories and the flow fields are computed for various hovering altitudes and dust grain sizes. Comparisons are made to Robert's original predictions and Apollo photogrammetry [4].

**Keywords:** Plume Impingement, Hybrid Continuum-DSMC, Particle-Laden Flows

**PACS:** 47.45.Dt, 52.20.Hv, 96.20.Ka, 47.61.Jd, 47.55.Kf

## INTRODUCTION

As a lunar lander approaches the surface, the rocket engine exhaust plume strikes the ground causing dust and larger debris to be dispersed into the flow field. During the Apollo moon landings, the dust erosion posed several operational hazards, including obscuration of the pilot's vision and degradation of mechanical components, damage to space suit seals, and clogging of thermal rejection systems. The Apollo 12 astronauts returned samples from the Surveyor III vehicle, located 163m from the lunar module, LM, landing site. Surveyor was found to be covered with dust produced by the LM rocket blast and its surface was found to have small pits due to blast abrasion [5]. Lunar dust is particularly difficult to handle because it consists of a fine powder that is exceptionally rough at the microscopic scale. This occurs because the powdery dirt is formed by micrometeorite impacts which pulverize the soil into highly pitted and irregular grain shapes. The result of this action is a dust that has the ability to cling to nearly any surface it touches. Upon return to the LM after moon walks, dust clouds and respiratory problems in the crew cabin were reported by Apollo astronaut Gene Cernan. The Apollo lunar module was powered by a 10,000 lb thrust descent engine with a specific impulse of 311 s [6]. According to radio call outs during the Apollo 11 landing, lofted dust was first observed at an altitude of 20 m. After landing, the astronauts examined the area underneath the LM and found that the engine scoured a shallow crater ~3 cm deep [7]. In addition, video photogrammetry of the LM descent tapes indicates that the dust ejection angle with respect to the surface was approximately 2 degrees. Such issues were recognized early in the lunar exploration program and have been investigated over the years.

Modeling this process is broken into three different phases: solving for the rocket plume impinging on a solid surface, predicting how much dust is consequently lofted into the flow field, and tracking the resulting two phase dust spray. When the rocket plume impinges on the lunar surface, the expanded flow is processed by a strong surface shock. Downstream of the surface shock, there is a stagnation region directly under the engine bell and the strong favorable pressure gradient turns the flow outward creating a high velocity jet tangential to the surface. To solve for the flow field, a loosely coupled continuum to DSMC flow solver was used. This approach has been implemented successfully for 2D and 3D cases with surface craters [8]. In [9], the flow field was simplified by

assuming free molecular flow from the rocket engine. After solving for the flow field near the surface an entrainment model was used to predict how much dust is lofted into the flow field. Roberts developed a model to predict how much dust and which size grains would be lofted into the flow field [2]. He treated the rocket engine as a point source of momentum and calculated an erosion rate based on the shear stress on the surface and cohesive strength of the soil. Roberts also estimated the velocity at which the dust particles are ejected from the surface based on the particle diameter, thrust level, and altitude. He did not solve for the aerodynamic forces on the dust grains and alternatively assumed that the particles followed ballistic trajectories. Recent improvements have been made to Roberts' theory [3], and a number of different erosion mechanisms have been identified in [10, 11]. The dust spray is dominated by the aerodynamic forces once dust is entrained into the flow field, and Lagrangian tracking has been used to model the two phase flow in [12]. In the current work, dust grains are treated as a separate species in DSMC in much the same way that any other molecular species is handled.

## METHOD

In the current approach the flow field is first solved using a hybrid continuum and DSMC solver. From the resulting continuum flow field surface shear forces are determined and the flux of dust particles from the surface is computed using a slightly modified version of Roberts' theory. These dust grains are subsequently injected into the DSMC flow field and their trajectories and velocities are mapped.

### Plume Impingement

The entire computational domain is first solved to steady state with the continuum flow solver, DPLR. We consider the scenario where the rocket engine hovers at a fixed altitude and is directed normal to the surface, Fig. 1. The computational domain is bounded by a specified inflow at the nozzle exit plane, a constant temperature wall at the lunar surface, a symmetry boundary condition along the engine centerline, and supersonic exit conditions everywhere else. Although the macroscopic properties at the exit plane of a real nozzle are non-uniform and a thin boundary layer exists, constant properties across the exit plane are assumed. A constant lunar surface temperature of 1000 K is used in the following simulations. The LM descent engine burned Aerozine-50 and nitrogen tetroxide and the exhausting gas mixture contained many different species, mainly  $\text{NH}_3$ ,  $\text{H}_2\text{O}$ ,  $\text{CO}$ ,  $\text{NO}$ ,  $\text{O}_2$ ,  $\text{CO}_2$ , and  $\text{NO}_2$  [6]. For our current simulations ammonia is used as the representative species.

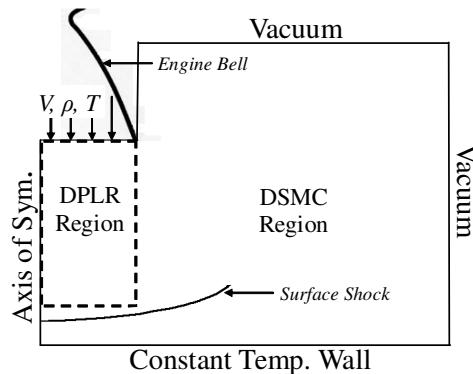


**FIGURE 1.** Computational domain and boundary conditions. The hybrid interface is marked by the dashed rectangle.

The DSMC and continuum solvers are coupled using volume reservoir cells [14]. An interface between the DSMC and continuum calculations is drawn in the cylindrical shell from the nozzle exit plane to a height slightly above the surface shock. At this location the interface normal Mach number is supersonic and the flow is largely continuum. Molecules are generated in creation cells along this prescribed interface with macroscopic properties specified by the DPLR solution. The creation cells are populated at each time step by DSMC particles generated from the corresponding Maxwellian distribution functions. A Maxwellian distribution is used instead of the Chapman-Enskog distribution because in this region the flow is nearly inviscid and the flow gradients are relatively small. Once moved, the molecules that have not entered the computational domain or reside inside of a creation cell

are deleted. Once inside of the DSMC domain, the molecules are treated as traditional DSMC particles that undergo translational and rotational energy exchange. Vibrational energy is ignored in the examples presented.

## Dust Generation and Transport

Metzger has identified three possible erosion mechanisms: viscous erosion, bearing capacity failure, and diffused gas eruption [10-11]. Viscous erosion occurs when the surface shear exceeds the cohesive strength of the soil and small dust particles begin to roll along the surface. The rolling dust grains can collide with neighboring particles and may then be lofted into the flow field. Bearing capacity failure occurs when the pressure exceeds the bearing capacity of the soil and a narrow cup is formed. The walls of the narrow cup are unstable and collapse, releasing many dust grains into the flow field while forming a wider crater. The third mechanism is diffused gas eruption; this occurs when the gas is driven into porous spaces and consequently moves a slab of dust instead of a thin dust layer described by viscous erosion. Due to the high packing density and bearing strength of lunar soil, bearing capacity failure is neglected as a dust generating mechanism. We do not consider flow through porous media in our simulations and only consider viscous erosion as the dominant dust producing mechanism. This is the same mechanism that Roberts used when developing his theory. The mass flux of dust grains is computed from eq. 1. The product  $au$  is the fraction of the local gas velocity at the boundary layer edge that a dust particle is ejected at,  $dm/dt$  is the particle mass flux per unit area, and  $\tau$  and  $\tau_c$  are the shear stress and shear strength of the soil respectively.

$$\frac{1}{2} au \frac{dm}{dt} = \tau - \tau_c \quad (1)$$

The coefficient  $a$  is obtained from:

$$a = \left[ \frac{1}{2} + \sqrt{\frac{1}{4} + \frac{1}{\zeta}} \right]^{-1} \quad (2)$$

$$\zeta = \frac{18\mu_c h}{\sigma\sqrt{RT_c}(4+k_h)} \left[ \frac{1}{D^2} + \frac{1}{D} \frac{(4+k_h)C_d F}{72e\sqrt{2RT_c}\mu_c} \right] \quad (3)$$

where  $\mu_c$  and  $T_c$  are the rocket chamber viscosity and temperature,  $h$  is the altitude of the engine,  $k_h$  is the hypersonic factor  $\gamma(\gamma-1)M_n^2$ ,  $\sigma$  and  $D$  are the dust particle's density and diameter,  $F$  is the engine's thrust, and  $C_d$  is a drag coefficient (assumed 0.2 by Roberts) on an individual dust grain. The Mach number at the exit plane of the nozzle is  $M_n$  and the ratio of specific heats is  $\gamma$ . The shear strength of the soil is defined as

$$\tau_c = c + P \tan \varphi \quad (4)$$

where  $c$  is the cohesive stress,  $P$  is the pressure, and  $\varphi$  is the friction angle. Mechanical properties of the soil are obtained from [13], and in our simulation we assume that the cohesive stress is 100 Pa and the friction angle is 30°. One can compute the surface shear stress by assuming a laminar or turbulent boundary layer if the surface roughness is small relative to the boundary layer thickness. Alternatively, if the surface roughness is not negligible compared to the boundary layer height, the shear stress can be computed by using the local dynamic pressure at the upper edge of the boundary layer and an assumed drag coefficient. Using the dynamic pressure to compute the shear stress is the most conservative assumption and results in loads much larger than laminar or turbulent shear stress. In our simulations, the local dynamic pressure and an assumed drag coefficient of 1.0, suggesting roughness scales comparable to the boundary layer thickness, yields an erosion rate that agrees well with the observed Apollo landings. Roberts' theory accounts for the aerodynamic forces on the dust grains by computing an initial ejection velocity,  $au$ , assuming an ejection angle and assuming ballistic trajectories. Since dust grains in our model are coupled to the flow field and are accelerated by collisions with the gas, the particles are injected with a zero initial velocity. The sensitivity of the solution to the initial particle velocity is discussed later in this report.

To couple the dust grains to the gas, we treat the grains as a hard sphere species with a large molecular mass and diameter. The collision cross section between dust grains and the gas is relatively large and a collision weighting scheme is implemented to reduce the computational effort. Without collision weighting each DSMC gas molecule may have to collide thousands of times with each dust grain. Alternatively, the number of collisions can be reduced by a factor  $N$  by temporarily scaling the mass of the gas molecule by  $N$ . By increasing the mass of the gas molecule, many collisions with a less massive gas molecule are replaced with fewer collisions with a heavier gas molecule. In addition, we are currently assuming a low mass fraction of dust grains and do not update the velocities of the gas during a collision with a dust particle. When dust grains strike the surface they impact other dust grains and can

cause more dust particles to enter the flow. This process is called saltation and is neglected in the current work. In our model the dust grains that strike the wall are diffusely reflected.

## NUMERICAL RESULTS

We present results for a 10,000lb thrust engine with an exit plane diameter of 1 m at three different altitudes: 5 m, 10 m, and 15 m. The density, temperature, and velocity at the exit plane of the nozzle are  $0.0063 \text{ kg/m}^3$ , 556 K, and 3008 m/s. The exhausting gas is ammonia and the exit Mach number is 5. Figure 2 shows number density and translational temperature contours from pure DPLR and the hybrid solver when the rocket engine is at an altitude of 5 m.

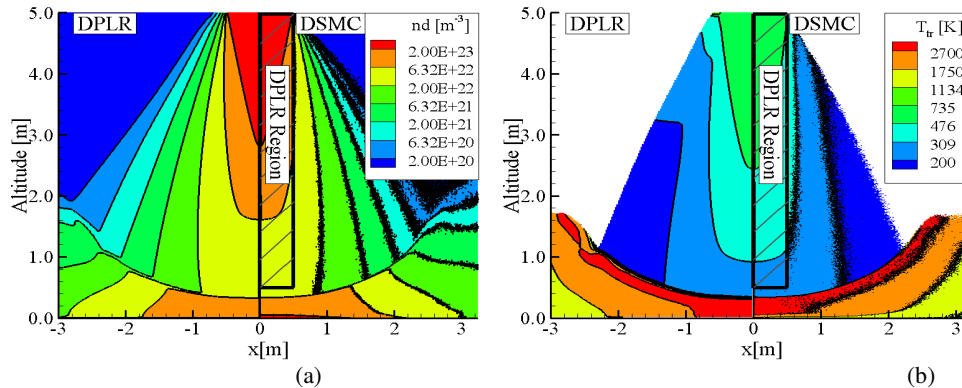


**FIGURE 2.** (a) Number density for the hybrid continuum solution. The left half is pure DPLR and the right half is hybrid. The hybrid interface is marked by the rectangle surrounding the hash-marked region. (b) Translational temperature for the same case.

The hybrid solution and continuum solution are similar outside of the boundary layer and the shock stand-off distance agrees well. Although the boundary layer in the DSMC solution is under-resolved, this is not critical because the surface shear stresses are computed from the DPLR solution and the dust grain trajectories are dominated by the gas flow outside of the boundary layer. At a hovering altitude of 5 m, the impinging flow is largely continuum and the interface in figure 2 is located where the breakdown parameter is small,  $O(10^{-4})$ , (see figure 3a). Beneath the surface shock wave the flow is highly collisional and consequently very computationally expensive. To reduce the computational effort, a collision limiter that stops collisions from occurring once the flow is in equilibrium is used. Although it is more computationally efficient to use DPLR below the shock wave, problems arise due to the one-way coupling because the normal flow is subsonic. Figures 3b and 3c shows two different hybrid interfaces when the rocket engine is at an altitude of 10 m that yield glitches. In figure 3b, the interface is a cylindrical shell that extends from the ground to the nozzle exit. In figure 3c, the interface is constructed with two concentric cylindrical shells, one 3 m diameter shell near the surface and a 1 m diameter shell slightly above the surface shock wave. Even though the breakdown parameter indicates continuum flow at these interfaces, the inability of the DSMC simulation to feed back into the DPLR simulation results in errors.

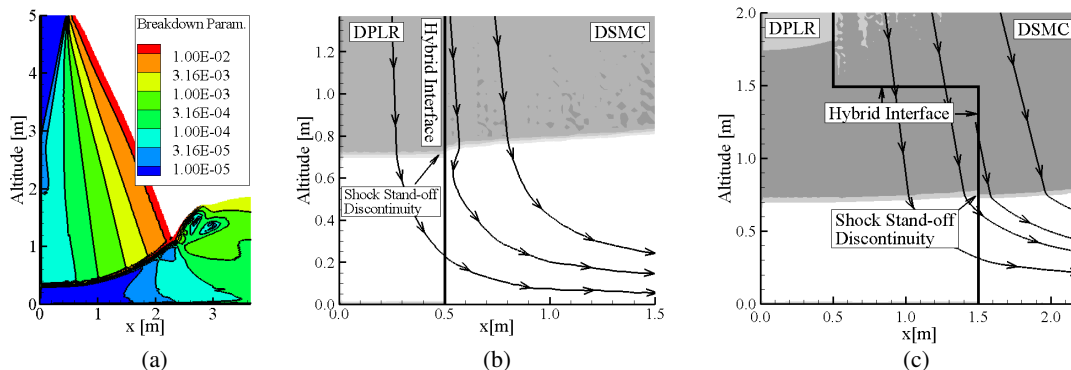


**FIGURE 3.** (a) Bird's breakdown parameter computed using the DPLR solution. (b) Cylindrical hybrid interface and flow streamlines. (c) A hybrid interface consisting of two concentric cylinders and the corresponding streamlines.

In figure 3b, the DSMC streamlines near the interface non-physically deflect towards the axis of symmetry because there is a discontinuity in the shock stand-off distance between the two solvers. DPLR predicts a surface shock that rests slightly closer to the surface than the DSMC prediction. Consequently the DSMC particles immediately downstream of the shock see a low pressure boundary condition at the continuum interface and the streamlines are deflected inward. In figure 3c, the shock stand-off distance in DPLR is larger than that for DSMC and the streamlines are deflected slightly to the right.

The erosion rates were determined from the DPLR solution assuming a 30 micron dust diameter. Particle entrainment first occurs at an altitude near 15 m and Apollo observations report dust entrainment at altitudes ranging from 18 m to 30 m. Better agreement is not expected because the LM axis was not oriented normal to a single point on the surface and the local surface topography is not modeled. During the Apollo 11 landing, the astronauts observed that the LM descent engine excavated a shallow 3 cm crater. An approximate descent trajectory was reconstructed from Buzz Aldrin's radio callouts. We further approximate the descent trajectory by using three different altitudes, 5 m, 10 m, and 15 m, with the LM spending 20 s at each altitude. The shear stresses, particle mass fluxes, and predicted crater depth are shown in figure 4.

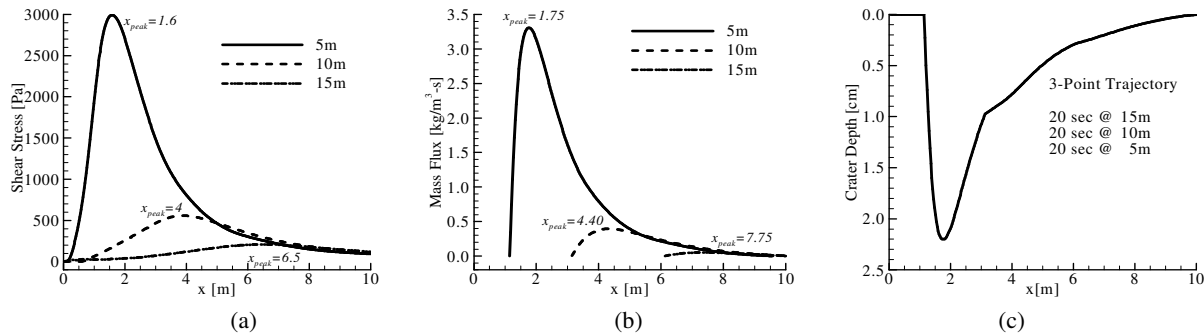


**FIGURE 4.** (a) Surface shear stress distribution plotted at three different altitudes. (b) The particle mass flux plotted at three different altitudes. (c) The predicted crater depth based on an assumed three point trajectory.

Roberts' theory predicts maximum surface shear stresses that are consistently less than the values predicted from DPLR, table 1. The discrepancies are larger at lower altitudes because Roberts' density profiles assume a point source of momentum and at low altitudes this assumption is far from valid. Additionally, Roberts' theory predicts the maximum shear stress on the surface to be located at a distance  $h$  from the axis of symmetry where  $h$  is the altitude of the rocket engine. Our simulations indicate the maximum shear stress occurs 1.6 m, 4 m, and 6.5 m from the axis of symmetry at altitudes of 5 m, 10 m, and 15 m: roughly  $h/2$ . The location of peak mass flux is further from the axis than peak surface shear because at further distances the pressure and soil shear strength diminish.

**TABLE 1.** Maximum shear stress computed from Robert's theory and DPLR.

Altitude [m]	Max. Shear Stress - Roberts [Pa]	Max. Shear Stress - DPLR [Pa]
5	1542	2995
10	385	590
15	171	190

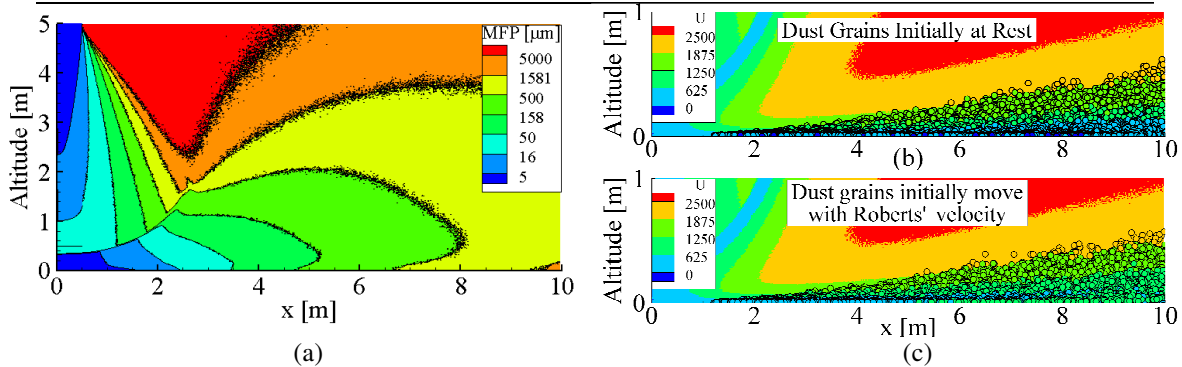


**FIGURE 5.** (a) 30 micron diameter dust particles overlaid upon the gas mean free path. (b) Horizontal velocity of gas and dust grains. The dust grains are initially at rest. (c) Dust grains are initially ejected with a velocity determined by Roberts' theory.

From the computed mass flux distribution, dust grains are generated at the surface each time step with a zero initial velocity, figure 5a. The dust grains have an assumed diameter of 30 microns, particle density of  $3000 \text{ kg/m}^3$ , and a roundness of 0.1 [13]. The roundness is the ratio of the mean diameter of the dust grain to the diameter of the sphere that circumscribes the entire particle. Since the dust grains are not spherical, the volume of the particle is computed from the mean diameter and the cross section is computed from the maximum diameter of the particle. Near the surface where the dust grains are first generated, the particle diameter is on the same order of magnitude or smaller than the mean free path of the gas. Consequently it is not valid to use Stokes drag approximations and a transitional or free molecular approach is necessary. At a distance 10 m from the axis of symmetry the dust particles have a mean ejection velocity of 1700 m/s and the spray is inclined at  $2.8^\circ$ . The initial particle velocity does not affect the trajectories because they are rapidly accelerated by the aerodynamic forces, figures 5b and 5c.

## CONCLUSIONS

Rocket plume impingement flow fields have been solved using a loosely coupled continuum – DSMC model for rocket altitudes of 5 m, 10 m, and 15 m. Qualitatively the continuum and hybrid solutions are similar, and good agreement is found in the shock stand-off distance. Viscous erosion is assumed to be the dominant mechanism for dust entrainment because the lunar soil has a high packing density and bearing capacity. Dust erosion rates were estimated by applying Roberts' theory of dust entrainment in the continuum flow field. It is found that dust erosion for the LM descent engine occurs at an approximate altitude of 15 m and based on a 3-point trajectory the excavated crater depth is approximately 2 cm deep. These predictions agree with Apollo observations. When the rocket engine is 5 m off the surface, a high-velocity dust spray is inclined at  $2.8^\circ$ . The 30 micron diameter dust spray has a mean velocity of 1700 m/s at a distance 10 m and the trajectories are insensitive to initial velocity.

## ACKNOWLEDGMENTS

This work has been supported by NASA LASER grant NNX08AW08G.

## REFERENCES

1. M. J. Wright, G. V. Candler, and D. Bose", *AIAA Journal*, Vol. 36, No. 9, pp. 1603-1609, Sep. 1998.
2. L. Roberts, "The Interaction of a Rocket Exhaust With the Lunar Surface", *The Fluid Dynamic Aspects of Space Flight, AGARDograph 87*, Vol. II, Gordon & Breach, 269-290, 1966.
3. P. T. Metzger et al., "Modification of Roberts' Theory for Rocket Exhaust Plumes Eroding lunar Soil", presented at the 11<sup>th</sup> ASCE Aerospace Division International Conference on Engineering, Science, Construction, and Operation in Challenging Environments, Long Beach, CA, 3-5 March 2008.
4. C. Immer et al., "Apollo Video Photogrammetry Estimation of Plume Impingement Effects", presented at the 11<sup>th</sup> ASCE Aerospace Division International Conference on Engineering, Science, Construction, and Operation in Challenging Environments, Long Beach, CA, 3-5 March 2008.
5. J. R. Gaier, "The Effects of Lunar Dust on EVA Systems During the Apollo Missions", NASA/TM-2005-213610, NASA Glenn Research Center, Cleveland, OH 2005.
6. B. R. Simoneit, et. al., "Apollo Lunar Module Engine Exhaust Products", *Science*, **166**, No. 3906, pp. 733-738, 1969.
7. C. C. Mason, "Comparison of Actual Versus Predicted Lunar Surface Erosion Caused by Apollo 11 Descent Engine", *Geological Society of America Bulletin*. **81**, 1807-1812 (1970).
8. F. Lumpkin et al., "Plume Impingement to the Lunar Surface: A Challenging Problem for DSMC", presented at the *Direct Simulation Monte Carlo, Theory, Methods, and Applications Conference*, Santa Fe, NM, 30 Sept – 3 October 2007.
9. M. Woronowicz, "Modeling of Lunar Dust Contamination Due to Plume Impingement", presented at the 6<sup>th</sup> International Planetary Probe Workshop, Atlanta, GA, 25 June 2008.
10. P. T. Metzger et al., *J. Aero. Eng.* **22**, 24-32 (2009).
11. P. T. Metzger et al., "Craters Formed in Granular Beds by Impinging Jets of Gas" in *Powders and Grains-2009: Proc. of the 6<sup>th</sup> Intern. Conf. on Micromechanics of Gran. Media*, edited by M. Nakagawa et al., AIP Conf. Proc. 1145, 767-770 (2009).
12. J. E. Lane et al., "Lagrangian Trajectory Modeling of Lunar Dust Particles", presented at the 11<sup>th</sup> ASCE Aerospace Division International Conference on Engineering, Science, Construction, and Operation in Challenging Environments, Long Beach, CA, 3 March 2008.
13. G. Heiken, D. Vaniman, and B. M. French, *Lunar Sourcebook*, New York: Cambridge University Press, 1991, pp. 475-594.
14. R. Roveda, D. Goldstein, P. Varghese, in *Proc. of the 21st Rarefied Gas Dynamics Conference*, **2**, pp 117-224, 1998.